AD-A054 860 IOWA UNIV IOWA CITY DEPT OF PHYSICS AND ASTRONOMY F/G 3/2

ION ACOUSTIC WAVES IN THE SOLAR WIND, (U)

APR 79 D A GURNETT, L A FRANK NAS5-11279

UNCLASSIFIED NL

1 OF 2

AD A054860

END

DATE FILMED

7-78

DDC

CONT

VOL. 83, NO. A1 JOURNAL OF GEOPHYSICAL RESEARCH JANUARY 1, 1978

Ion Acoustic Waves in the Solar Wind

D. A. GURNETT AND L. A. FRANK

Department of Physics and Astronomy, University of Iowa, Iowa City, Iowa 52242

Plasma wave measurements on the Helios 1 and 2 spacecraft have revealed the occurrence of electric field turbulence in the solar wind at frequencies between the electron and ion plasma frequencies. Wavelength measurements with the Imp 6 spacecraft now provide strong evidence that these waves are short-wavelength ion acoustic waves which are Doppler-shifted upward in frequency by the motion of the solar wind. Comparison of the Helios results with measurements from the earth-orbiting Imp 6 and 8 spacecraft shows that the ion acoustic wave turbulence detected in interplanetary space has characteristics essentially identical to those of bursts of electrostatic turbulence generated by protons streaming into the solar wind from the earth's bow shock. In a few cases, enhanced ion acoustic wave intensities have been observed in direct association with abrupt increases in the anisotropy of the solar wind electron distribution. This relationship strongly suggests that the ion acoustic waves detected by Helios far from the earth are produced by an electron heat flux instability, as was suggested by Forslund. Possible related mechanisms which could explain the generation of ion acoustic waves by protons streaming into the solar wind from the earth's bow shock are also considered.

Introduction

Plasma wave measurements on the solar-orbiting Helios 1 and 2 spacecraft [*Gurnett and Anderson*, 1977] have recently revealed the occurrence of significant levels of electric field turbulence in the solar wind at frequencies from about 1 to 10 kHz, between the electron and ion plasma frequencies. In this paper we expand the initial investigation of this turbulence and present evidence that this turbulence consists of short-wavelength ion acoustic waves below the ion plasma frequency which are Doppler-shifted upward in frequency by the motion of the solar wind. Measurements are presented both in interplanetary space, from Helios 1 and 2, and in the solar wind upstream of the earth's bow shock, from Imp 6 and 8. These data provide a comprehensive description of the spectrum, polarization, wavelength, and other essential characteristics of the turbulence. Comparisons are also made with the ambient plasma parameters under a variety of conditions to identify the origin of these waves. In interplanetary space, far away from the earth, the primary mechanism for producing the ion acoustic waves is believed to be the electron heat flux instability suggested by *Forslund* [1970]. Near the earth, however, the same types of waves are often observed to be associated with low-energy (1-10 keV) protons streaming toward the sun from the earth's bow shock. Thus more than one mechanism is apparently operative in the solar wind to destabilize the ion acoustic mode. As will be discussed, similar mechanisms, based on an induced drift between the solar wind electrons and protons, are believed to account for both the heat flux and the proton streaming instabilities.

In the initial description of the ion acoustic wave turbulence by *Gurnett and Anderson* [1977] this turbulence was called $f_p^+ < f < f_p^-$ noise. This terminology was chosen on a strictly observational basis, since the largest intensities usually occur in the frequency range between the electron and ion plasma frequencies f_p^- and f_p^+. As detected by Helios 1 and 2, the maximum single-channel (±10% bandwidth) electric field amplitudes of the $f_p^+ < f < f_p^-$ noise are typically a few hundred microvolts per meter. The electric field strength of this noise is very impulsive, consisting of many brief bursts lasting for only a few seconds. When it is viewed on a time scale of several hours or more, the $f_p^+ < f < f_p^-$ noise is present a large fraction (30–50%) of the time. The noise is observed over the entire range of the Helios orbits from about 0.3 to 1.0 AU. The frequency spectrum of the $f_p^+ < f < f_p^-$ noise shows a systematic variation with radial distance from the sun, shifting toward higher frequencies closer to the sun. Spin modulation measurements show that the electric field of the noise tends to be aligned along the direction of the magnetic field in the solar wind. Gurnett and Anderson discussed the possible plasma wave modes which could account for the $f_p^+ < f < f_p^-$ noise and concluded that the noise could be produced by either the *Buneman* [1958] mode or the ion acoustic mode, the ion acoustic mode being the most likely.

Helios Observations in Interplanetary Space

Since more data have now been analyzed from the Helios plasma wave experiments, a much more detailed analysis of the $f_p^+ < f < f_p^-$ noise detected by Helios in the interplanetary medium can be provided than was given in the initial survey by *Gurnett and Anderson* [1977]. For details of the Helios 1 and 2 plasma wave instrumentation, see the paper by *Gurnett and Anderson* [1977]. A typical example of the $f_p^+ < f < f_p^-$ noise detected by Helios 2 is shown in Figure 1. Helios 2 at this time is near the earth-sun line at a heliocentric radial distance of about 0.45 AU. The solid lines for each frequency channel in Figure 1 show the peak electric field intensities over 40.0-s intervals, and the vertical bars (solid black areas) indicate the corresponding average electric field intensities. The intensity scales are logarithmic with a total range of 100 dB from the bottom of one channel to the bottom of the next adjacent channel. The $f_p^+ < f < f_p^-$ noise is evident as a broad band of noise extending from about 1.0 to 17.8 kHz, roughly between the electron and ion plasma frequencies f_p^- and f_p^+, as indicated on the right-hand side of Figure 1. A typical spectrum, selected from Figure 1 at a time of nearly maximum intensity, is shown in Figure 2. The broad peak in the spectrum between the electron and ion plasma frequencies is clearly evident. The relationship to the local electron and ion plasma frequencies $f_p^+ < f < f_p^-$ is believed to be mainly fortuitous, since as will be shown later, the frequency spectrum is strongly Doppler-shifted by the motion of the solar wind. Both Figure 1 and Figure 2 show that the peak field strengths of the $f_p^+ < f < f_p^-$ noise are much larger than the average field strengths, indicating that the noise is very impulsive. The detailed temporal

Paper number 7A0723.
0148-0227/78/017A-0723$03.00

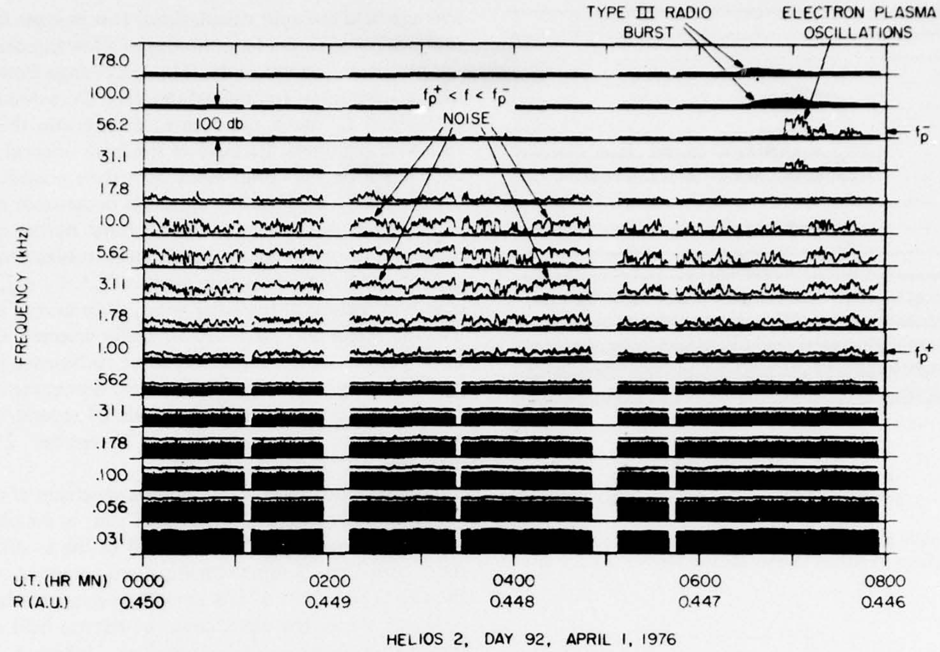

Fig. 1. Typical example of the $f_p^+ < f < f_p^-$ noise detected by the Helios 2 spacecraft at about 0.45 AU. The solid lines and the vertical bars (solid black areas) indicate the peak and average electric field strengths. The intense noise at low frequencies, $\lesssim$311 Hz, is caused by interference from the spacecraft solar array.

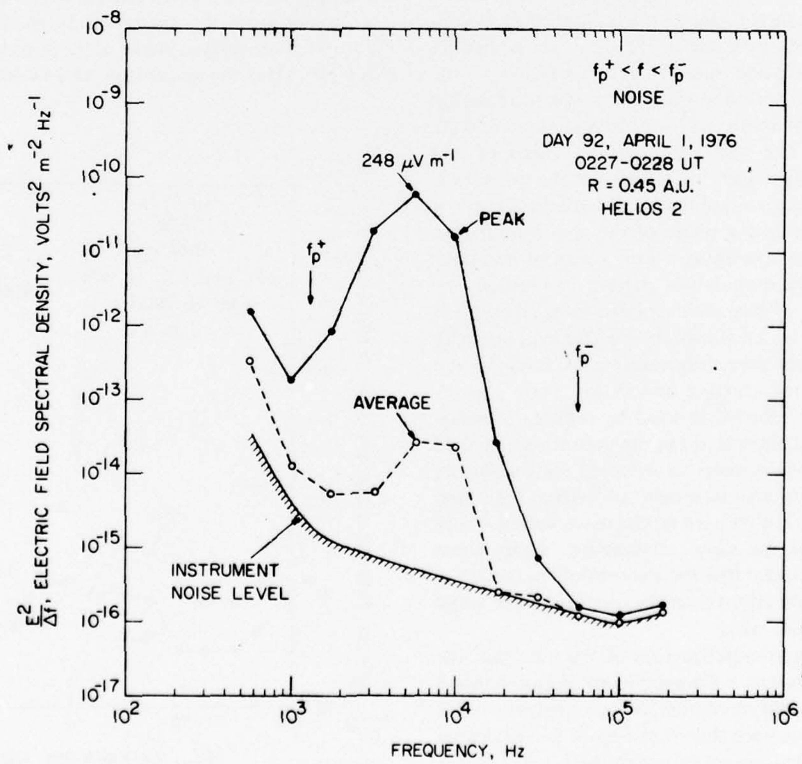

Fig. 2. Typical spectrum of the $f_p^+ < f < f_p^-$ noise at a selected interval from Figure 1. Note the distinct peak in the spectrum at about (2–10)f_p^+ and the large ratio of the peak to the average electric field strength, indicative of very impulsive temporal variations.

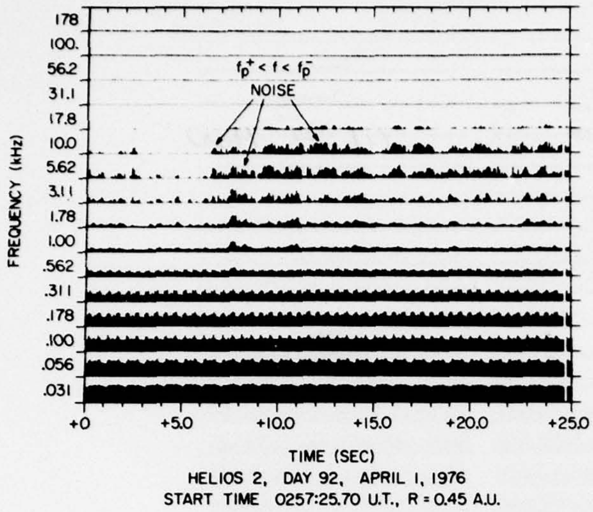

Fig. 3. Very high time resolution measurements from Figure 1, showing the impulsive burstlike temporal structure of the $f_p^+ < f < f_p^-$ noise.

variations are illustrated in Figure 3, which shows a very high time resolution snapshot of the electric field intensities stored in the spacecraft memory from the event in Figure 1, at about 0257 UT. These high time resolution measurements show that the $f_p^+ < f < f_p^-$ noise consists of many short bursts lasting only a few tenths of a second. The individual bursts have a very broad bandwidth and tend to occur simultaneously across a broad range of frequencies. Occasionally, high time resolution measurements, such as those in Figure 3, show distinct evidence of spin modulation caused by the rotation of the electric antenna. A brief period in which such spin modulation is apparent occurs from about +12 to +15 s in the 1.78-kHz channel in Figure 3. The spin modulation consists of two maxima and two minima in each 1-s rotation of the spacecraft. In most cases the extremely rapid temporal variations make it very difficult to determine the phase of the spin modulation accurately. However, by averaging a long series of measurements the detailed spin modulation pattern can usually be identified. An example of one such series of measurements is illustrated in Figure 4, which shows the electric field intensity distribution above a fixed percentage occurrence level (10 and 20%) as a function of the antenna orientation angle φ_{SE}^A. A long (1 hour) analysis interval is used to reduce statistical fluctuations. These data show that the maximum electric field intensity occurs when the antenna is oriented approximately parallel to the solar wind magnetic field. Individual high time resolution measurements of the spin modulation, such as those in Figure 3, also show the same relationship. From these measurements it is concluded that the electric field of the $f_p^+ < f < f_p^-$ noise is oriented approximately parallel to the static magnetic field in the solar wind.

To illustrate the approximate fraction of the time that the $f_p^+ < f < f_p^-$ noise is present in the solar wind, Figure 5 shows the peak and average field strengths for one complete solar rotation. The four frequencies shown in Figure 5 are selected to cover the range of frequencies in which the $f_p^+ < f < f_p^-$ noise is normally observed. Here, as in Figure 1, the peak and average field strengths are shown by lines and vertical bars. A time interval of 36.0 min is used for both the peak and the average field strength calculations. It is evident from Figure 5 that peak electric field amplitudes of a few hundred microvolts per meter are present in the frequency range from 1.78 to 5.62 kHz a substantial fraction of the time. Occasionally, bursts of $f_p^+ < f < f_p^-$ noise are seen to extend into the 562-Hz and 17.8-kHz channels. Because of the long interval for the peak determination the compressed time scale presentation in Figure 5 tends to enhance the apparent occurrence of the $f_p^+ < f < f_p^-$ noise, since even one short burst during any given 36-min interval will register in the peak measurements. Nevertheless, these data show that bursts of $f_p^+ < f < f_p^-$ noise are a common feature of the solar wind, since during any given 36-min interval a few bursts are normally detected. Occasionally, quiet periods occur. However, some turbulence is usually detected in any given 36-min interval. Sometimes, distinct enhancements are evident for periods of several days, for example, from November 21 to November 23 and from November 27 to November 29.

To investigate the variation in the spectrum of the $f_p^+ < f < f_p^-$ with radial distance from the sun, a detailed statistical analysis has been performed on all of the available Helios 1 data, consisting of approximately two complete orbits around the sun. The results of this analysis are summarized in Figure 6, which shows the distribution of electric field strengths detected in each frequency channel as a function of radial distance. The electric field strengths used in this analysis are 36-min peak values, comparable to those in Figure 5. The electric field strength contours shown in Figure 6 correspond to intensities which are exceeded a fixed fraction (5 and 10%) of the time. The portion of the overall spectrum attributed to the $f_p^+ < f < f_p^-$ noise is indicated by the shaded areas. The steeply rising spectrum at low frequencies ($\lesssim$500 Hz) is caused by interference from the spacecraft solar array (also evident in Figure 1). The isolated peaks in the spectrum at high frequencies ($\gtrsim$30 kHz) are caused by narrow-band electron plasma

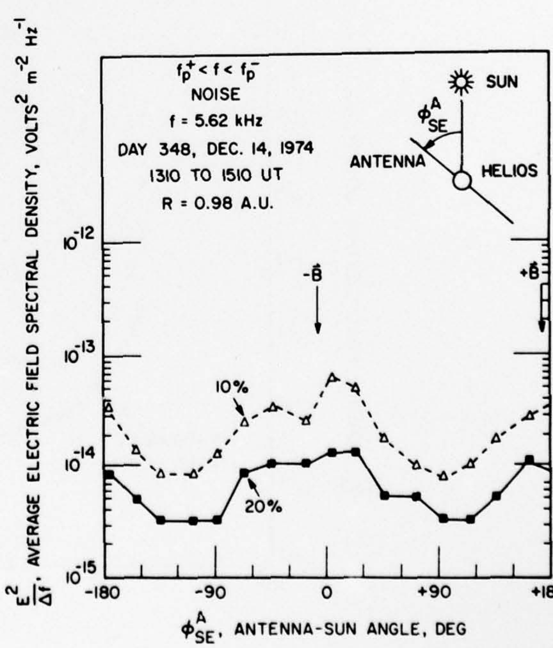

Fig. 4. Angular distribution of the electric field intensity of the $f_p^+ < f < f_p^-$ noise, showing that the electric field of this noise is oriented approximately parallel to the solar wind magnetic field.

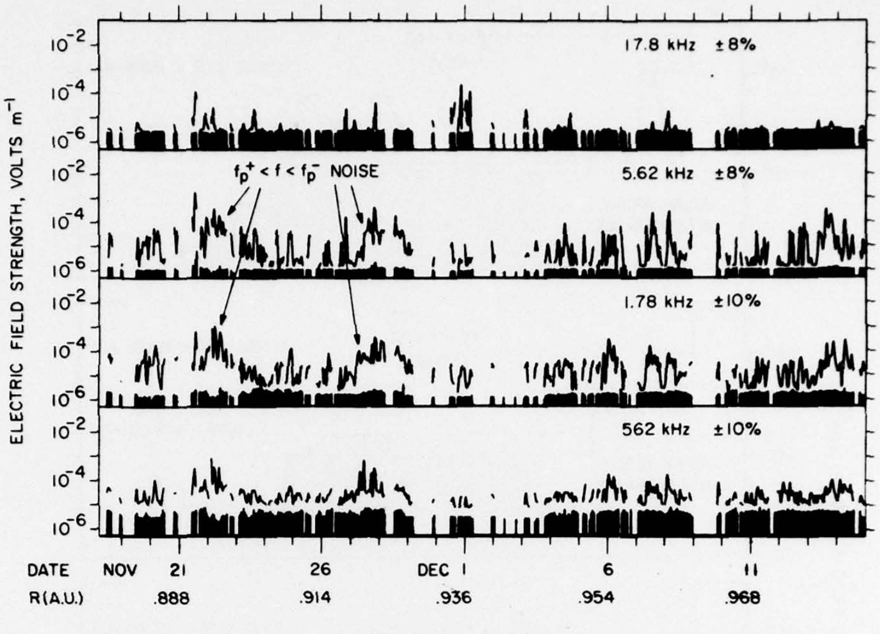

Fig. 5. Compressed time scale plot showing the electric field intensities for one solar rotation. Each peak and each average point represent a 36-min interval. These data show that a low level of $f_p^+ < f < f_p^-$ noise, at amplitudes of 10–100 μV m^{-1}, is present in the solar wind a substantial fraction of the time.

oscillations comparable to the event in Figure 1 at about 0700 UT. These plasma oscillations are directly associated with energetic electrons streaming outward from the sun [*Gurnett and Frank*, 1975] and are often directly associated with type III solar radio bursts [*Gurnett and Anderson*, 1976]. Although narrow-band electron plasma oscillations are easily distinguished from the $f_p^+ < f < f_p^-$ noise, no attempt was made to separate the two types of waves for the statistical analysis in Figure 6, since the plasma oscillations occur very infrequently. Figure 6 clearly shows that both the upper cutoff frequency and the intensity of the $f_p^+ < f < f_p^-$ noise increase with decreasing radial distance from the sun. A rough analysis indicates that the upper cutoff frequencies of the $f_p^+ < f < f_p^-$ noise and the frequency of the electron plasma oscillations vary approximately as $1/R$, where R is the heliocentric radial distance. The radial variation of the $f_p^+ < f < f_p^-$ noise intensity is shown in more detail in Figure 7, which gives the distribution of broadband electric field strengths as a function of the radial distance from the sun. The broadband electric field strengths used in this analysis are calculated by integrating the individual 36-min peak electric field spectrums from 562 Hz to 31.1 kHz. As can be seen from Figure 6, the main contribution to the $f_p^+ < f < f_p^-$ noise spectrum usually occurs in this frequency range. The frequency of occurrence contours in Figure 7 clearly show the increase in the $f_p^+ < f < f_p^-$ noise intensity with decreasing radial distance from the sun. A best fit analysis of the broadband field strength as a function of the radial distance, a power law radial distance dependence being assumed, indicates that the electric field strength also varies approximately as $1/R$.

IMP 6 AND 8 OBSERVATIONS UPSTREAM OF THE EARTH'S BOW SHOCK

Waves essentially identical to the $f_p^+ < f < f_p^-$ noise detected by Helios are also commonly observed by the Imp 6 and 8 spacecraft in the solar wind upstream of the earth's bow shock. See the description by *Gurnett* [1974] of the plasma wave instrumentation on Imp 6 and 8. As will be shown, some of the $f_p^+ < f < f_p^-$ noise bursts detected by Imp 6 and 8 are clearly of terrestrial origin, whereas others appear to be of interplanetary origin, as is true in the Helios observations. Figures 8, 9, and 10 illustrate some typical examples of the $f_p^+ < f < f_p^-$ noise detected by Imp 8 upstream of the bow shock. Figure 8 shows an example of an earth-related event in which a burst of $f_p^+ < f < f_p^-$ noise, from about 0920 to 1115 UT, is closely associated with the arrival of a stream of low-energy protons from the earth's bow shock. The corresponding charged particle measurements from the University of Iowa low-energy proton-electron differential energy analyzer (Lepedea) on Imp 8 are shown in Plate 1. Details of this spectrogram display of the charged particle intensities and the Lepedea instrumentation are given by *Frank et al.* [1976]. The sunward streaming 1- to 10-keV protons associated with the $f_p^+ < f < f_p^-$ noise are clearly evident in the second, third, and fourth spectrograms from the top in Plate 1, between about 0920 and 1115 UT, in almost exact coincidence with the burst of $f_p^+ < f < f_p^-$ noise. These spectrograms represent viewing directions looking toward local evening, local midnight, and local morning, respectively. The direction of motion of the protons can also be seen from the sector spectrogram in Plate 1, which shows that the protons are streaming toward the sun with directions of arrival in the range $120° \lesssim \varphi_{SE}{}^L \lesssim 300°$ (solar ecliptic coordinates). Imp 8 at this time is located upstream of the earth at a local time of about 14.5 hours and a geocentric radial distance of about 41 R_E. The observed directions of arrival correspond closely with the expected directions of motion for particles originating from the vicinity of the earth. The velocity distribution function for these protons, measured along directions approximately parallel to the earth-sun line, is shown in Figure 11, along with the ambient solar

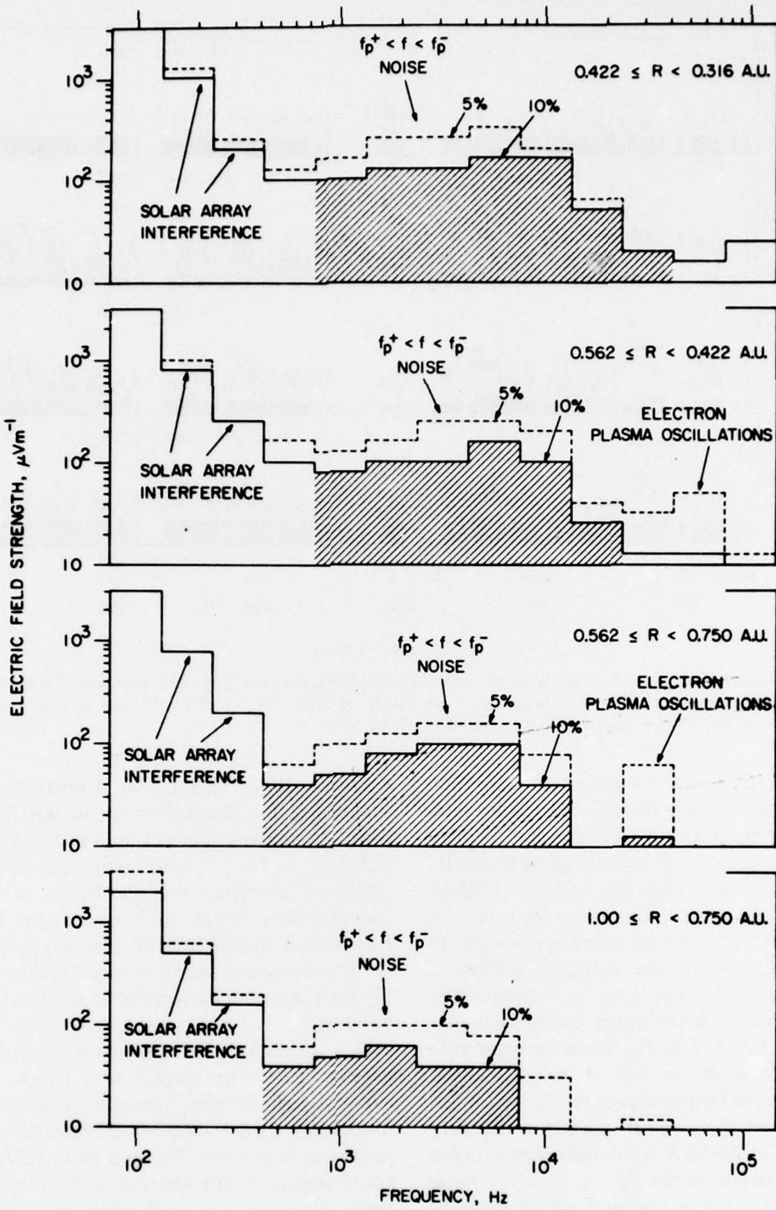

Fig. 6. Statistical survey of the 36-min peak field strength measurements of the type shown in Figure 5 for a total of two complete orbits around the sun. These data show that both the frequency and the amplitude of the $f_p^+ < f < f_p^-$ noise increase systematically with decreasing radial distance from the sun, with $f_{max} \propto 1/R$.

wind distribution determined from the Los Alamos plasma instrument on Imp 8 (W. Feldman, personal communication, 1977). As can be seen in Figure 11, the protons streaming into the solar wind produce a very pronounced double peak in the proton distribution function. Possible mechanisms by which these sunward streaming protons can generate $f_p^+ < f < f_p^-$ noise are considered later.

The upstream $f_p^+ < f < f_p^-$ noise associated with protons arriving from the earth's bow shock, such as that in Figure 8, almost certainly corresponds to the electrostatic noise first reported by *Scarf et al.* [1970] upstream of the bow shock from Ogo 5. In comparison to the $f_p^+ < f < f_p^-$ noise detected by Helios the upstream waves detected by Imp 8 have essentially identical characteristics. In both cases the noise is electrostatic and extends with comparable intensities from about 562 Hz to 10 kHz, between the electron and ion plasma frequencies. The peak electric field strengths are much greater than the average electric field strengths, as is true in the Helios measurements, and angular distributions, such as those in Figure 12, show that the wave electric field is aligned approximately parallel to the solar wind magnetic field, also in agreement with the Helios observations. From all available evidence the electrostatic waves generated upstream of the earth by protons arriving from the bow shock are essentially identical to the $f_p^+ < f < f_p^-$ noise detected by Helios far from the earth. These comparisons indicate that the same basic plasma wave mode is

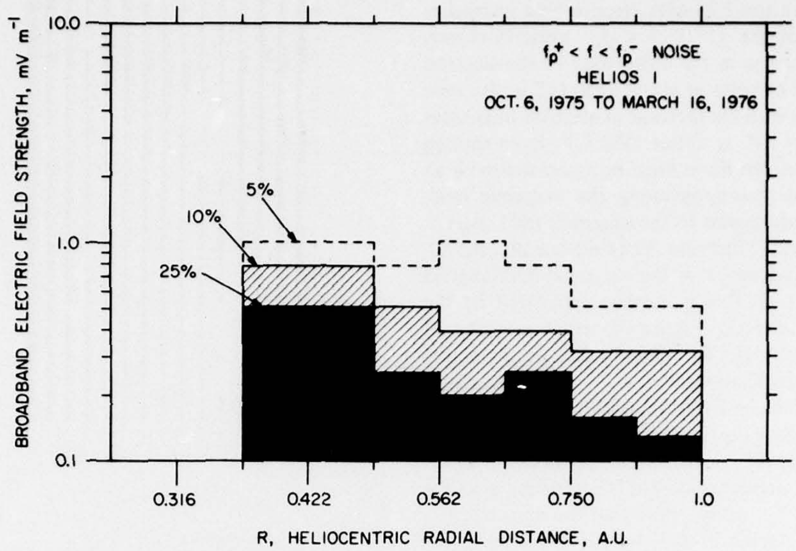

Fig. 7. More detailed analysis of the broadband electric field intensity as a function of the radial distance from the sun. The radial distance is plotted on a logarithmic scale, so that a power law dependence will be a straight line. The electric field amplitude varies approximately as $1/R$.

involved in both types of noise. The detailed mechanisms by which the noise is generated must, however, be quite different in the two cases, since protons from the earth's bow shock cannot possibly produce the waves detected by Helios far from the earth.

Not all of the $f_p^+ < f < f_p^-$ noise bursts detected by Imp 8 are associated with protons arriving from the bow shock. Figure 9, for example, shows a sequence of $f_p^+ < f < f_p^-$ noise events extending over an entire day which are not related to upstreaming protons. The corresponding Lepedea spectrograms in Plate 2 for the same day demonstrate that no sunward streaming protons are detectable during these events, except possibly for the event around 1300–1400 UT. The magnetic field during this day is often close to the ecliptic plane, so there is no possibility that the Lepedea, which scans viewing directions in the ecliptic plane, would not be able to detect protons streaming along the magnetic field from the bow shock. The corresponding electron spectrograms in Plate 2 also show no abrupt changes in the electron distribution function which can be clearly related to variations in the $f_p^+ < f < f_p^-$ noise intensity. Events of this type, for which no earth-related source can be identified, constitute about 30–50% of all of the $f_p^+ < f < f_p^-$ noise events detected by Imp 8 upstream of the bow shock. These events evidently correspond to the interplanetary $f_p^+ < f < f_p^-$ noise commonly detected by Helios far from the earth, since no earth-related source can be identified.

To try to identify the feature of the solar wind charged particle distribution which produces the interplanetary (non earth related) $f_p^+ < f < f_p^-$ noise, the Imp 8 Lepedea and plasma wave data have been examined for correlated events which would indicate the origin of the instability. Several events have been identified which strongly indicate that the anisotropy associated with the electron heat flux in the solar wind plays an important role in producing the $f_p^+ < f < f_p^-$ noise. One such event, which occurred during a disturbed period on July 5, 1974, is illustrated in Figure 10 and Plate 3. In this case a pronounced burst of $f_p^+ < f < f_p^-$ noise occurs from about 1645 to 1930 UT, preceded by a shorter burst from about 1540 to 1600 UT. The Lepedea spectrograms in Plate 3 clearly show that no protons are arriving from the earth's bow shock during this time, so these waves must correspond to the interplanetary $f_p^+ < f < f_p^-$ noise. The enhanced background, evident in the proton spectrogram throughout the period shown in Plate 3, is caused by an energetic solar cosmic ray event. Close examination of the electron sector spectrogram in the second panel from the bottom in Plate 3 shows that the $f_p^+ < f < f_p^-$ noise occurs during a period when a substantial anisotropy is present in the solar wind electron distribution. The maximum intensities occur for Lepedea viewing directions in the range $0° \lesssim \varphi_{SE}^L \lesssim 90°$, which are approximately symmetrical with respect to the magnetic field direction, $\varphi_{SE}^B \simeq 45°$, during this period. This anisotropy is representative of a substantial streaming of electrons along the magnetic field away from the sun. The electron velocity distribution indicates that these electrons correspond to the high-temperature 'halo' electrons which provide the main contribution to the heat flux in the solar wind [*Feldman et al.*, 1974]. The anisotropy evident in Plate 3 corresponds to an unusually large electron heat flux away from the sun, directed along the solar wind magnetic field. The detailed variations of the electron velocity distribution function at a fixed energy and the corresponding 1.78-kHz electric field intensity variations are shown in Figure 13 near the beginning of the event. The electron distribution function is shown in two directions, $\varphi_{SE}^L = 34°$ and $124°$, which are approximately parallel and perpendicular, respectively, to the average magnetic field directions projected onto the ecliptic plane during this period. The interpretation of these data is somewhat complicated by variations in the magnetic field direction. Before about 1610 UT the magnetic field is too far out of the ecliptic plane, $\theta_{SE}^B \gtrsim 60°$, for accurate measurements of the anisotropy parallel and perpendicular to the magnetic field. However, after about 1610 UT the magnetic field is sufficiently close to the ecliptic plane, $\theta_{SE}^B \lesssim 30°$, for good anisotropy measurements. As can be seen from Figure 13, after about 1650 the intensities at $\varphi_{SE}^L = 34°$, looking along the magnetic field toward the sun, increase substantially above the intensities at $\varphi_{SE}^L = 124°$, perpendicular to the magnetic field. Comparisons with the 1.78-kHz electric field intensities show that the onset of the $f_p^+ < f < f_p^-$ noise is closely correlated with the increase in the anisotropy of the electron distribution. The burst of noise at about 1550 UT is also seen to be correlated closely with the increase of electron intensities in the direction $\varphi_{SE}^L \simeq 34°$ at about 1552 UT. Even though θ_{SE}^B is large at this time, this burst must be associated with an anisotropic component streaming along the magnetic field, since the intensity perpendicular to the magnetic field, $\varphi_{SE}^L = 124°$, shows no comparable increase. The evidence that the $f_p^+ < f < f_p^-$ noise is associated with the magnetic-field-aligned anisotropy in the electron flux is further supported by the velocity distributions shown in Figure 14, which are selected for times when $\theta_{SE}^B \simeq 0°$ and for viewing directions parallel ($\varphi_{SE}^L = 304°$ and $34°$) and antiparallel ($\varphi_{SE}^L = 124°$ and $214°$) to the magnetic field. The electron intensity measurements at 1252 UT (triangles), before the onset of the $f_p^+ < f < f_p^-$ noise, show that the anisotropy is typically small, $\lesssim 20\%$, at all velocities. However, the measurements at 1720 UT (circles), after the onset of the $f_p^+ < f < f_p^-$ noise, show that the anisotropy is very large, typically a factor of 3–5, over a broad range of velocities. These velocity distributions also show that other than the change in the anisotropy the electron distribution functions are nearly identical in the two regions, before and after onset of the noise. Comparison of these velocity distributions with the measurements of *Feldman et al.* [1975] clearly identifies this anisotropy with a greatly enhanced heat flux of the halo electrons, directed along the magnetic field line away from the sun. These and other similar observations provide strong evidence that the anisotropy associated with the electron heat flux in the solar wind plays an essential role in the generation of these waves. Close inspection of the electron angular distributions in Plate 2 also shows, for example, that a similar electron anisotropy is present during the period when the ion acoustic waves in Figure 9 are being observed. The variations in the $f_p^+ < f < f_p^-$ noise intensity are not, however, as easily associated with changes in the electron distribution function in this case, possibly because the plasma is close to marginal stability, so that only very minor changes in the electron distribution or other parameters can trigger the growth or decay of the waves.

Identification of the $f_p^+ < f < f_p^-$ Noise as Short-Wavelength Ion Acoustic Waves

Some of the factors involved in the identification of the plasma wave mode associated with the $f_p^+ < f < f_p^-$ noise detected by Helios have already been discussed by *Gurnett and Anderson* [1977]. From the electrostatic character of the noise, all of the well-known electromagnetic modes of propagation, such as the whistler and magnetosonic modes, can be eliminated from consideration. The electric field orientation, parallel to the static magnetic field, further restricts the possibilities, eliminating, for example, the various types of ion cyclotron and Bernstein modes which propagate nearly perpendicular to the static magnetic field. Essentially only two plasma wave modes are known which could account for all of the observed characteristics. These modes are the ion acoustic mode at $f \lesssim f_p^+$ and the *Buneman* [1958] mode at $f_B \simeq (m^-/m^+)^{1/3} f_p^-$. We also note that *Scarf et al.* [1970] identified the same modes as the best candidates for explaining the upstream electrostatic noise, which is now believed to be the same basic plasma wave mode detected by Helios far from the earth. Although *Gurnett and Anderson* [1977] argue that it is unlikely that the proper conditions exist in the solar wind for generating the Buneman

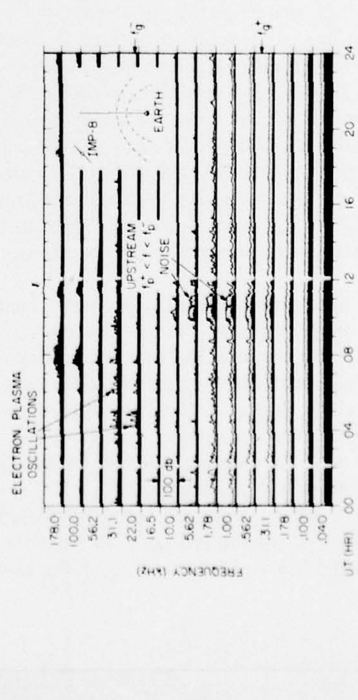

Fig. 8. Example of $f_p^+ < f < f_p^-$ noise detected upstream of the earth's magnetosphere in association with an intense burst of 1- to 10-keV protons streaming into the solar wind from the bow shock (see Plate 1).

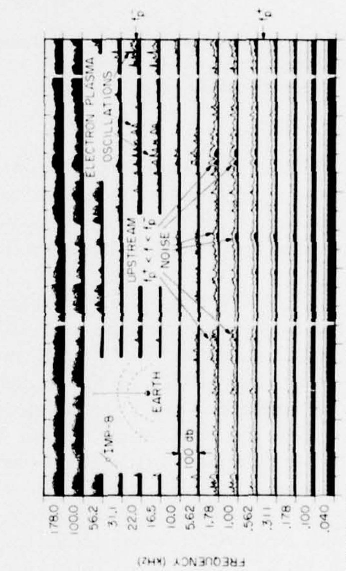

Fig. 9. Series of $f_p^+ < f < f_p^-$ noise bursts detected by Imp 8 for which no protons can be detected arriving from the bow shock (see Plate 2). These waves evidently correspond to the interplanetary $f_p^+ < f < f_p^-$ noise detected by Helios far from the earth.

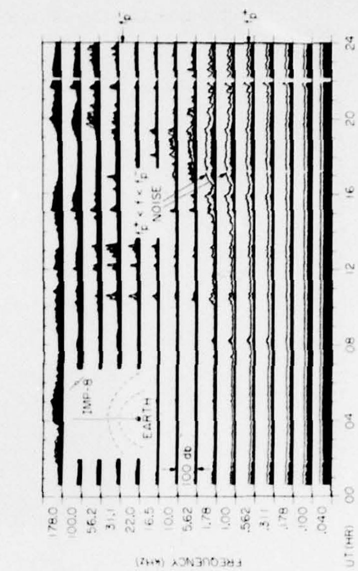

Fig. 10. Intense burst of $f_p^+ < f < f_p^-$ noise detected during a period when a substantial anisotropy is evident in the low-energy electron distribution (see Plate 3).

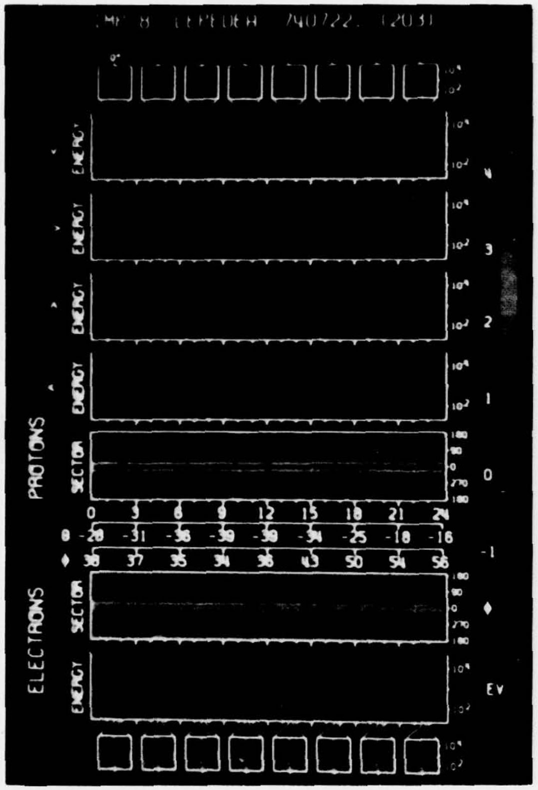

Plate 1. The Lepedea data corresponding to the electric field measurements in Figure 8, showing the occurrence of an intense burst of protons streaming toward the sun in direct correspondence with the burst of $f_p^+ < f < f_p$ noise from about 0920 to 1115 UT. These protons propagate from the earth's bow shock.

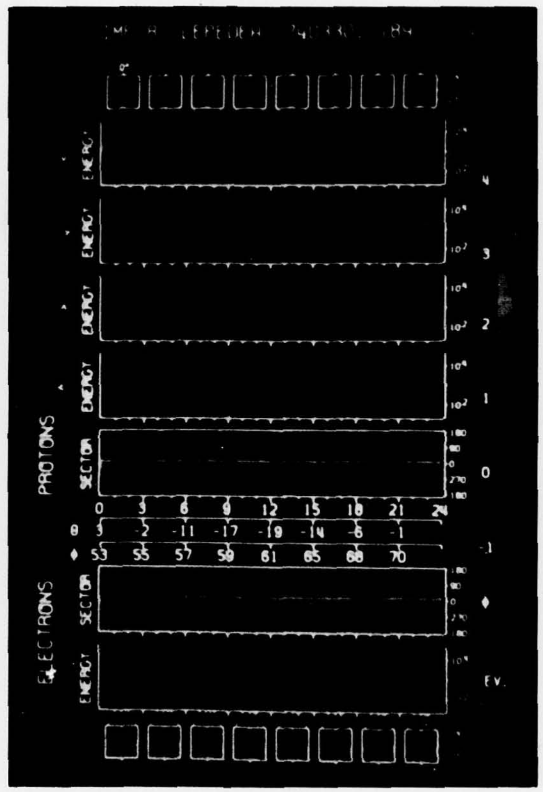

Plate 2. The Lepedea data corresponding to the electric field measurements in Figure 9, showing a series of $f_p^+ < f < f_p$ noise bursts for which no significant enhancement in either the electron or the proton intensities can be identified in association with the $f_p^+ < f < f_p$ noise.

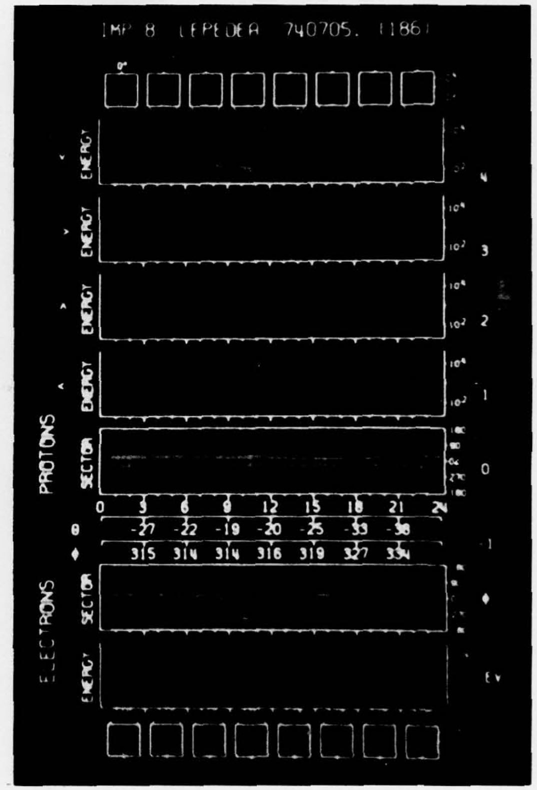

Plate 3. The Lepedea data corresponding to the electric field measurements in Figure 10, showing an event in which the $f_p^+ < f < f_p$ noise (from about 1540 to 1930 UT) is closely correlated with the occurrence of a greatly enhanced anisotropy in the low-energy solar wind electron distribution. This anisotropy is clearly evident in the electron sector spectrogram from about 1540 to 1900 UT.

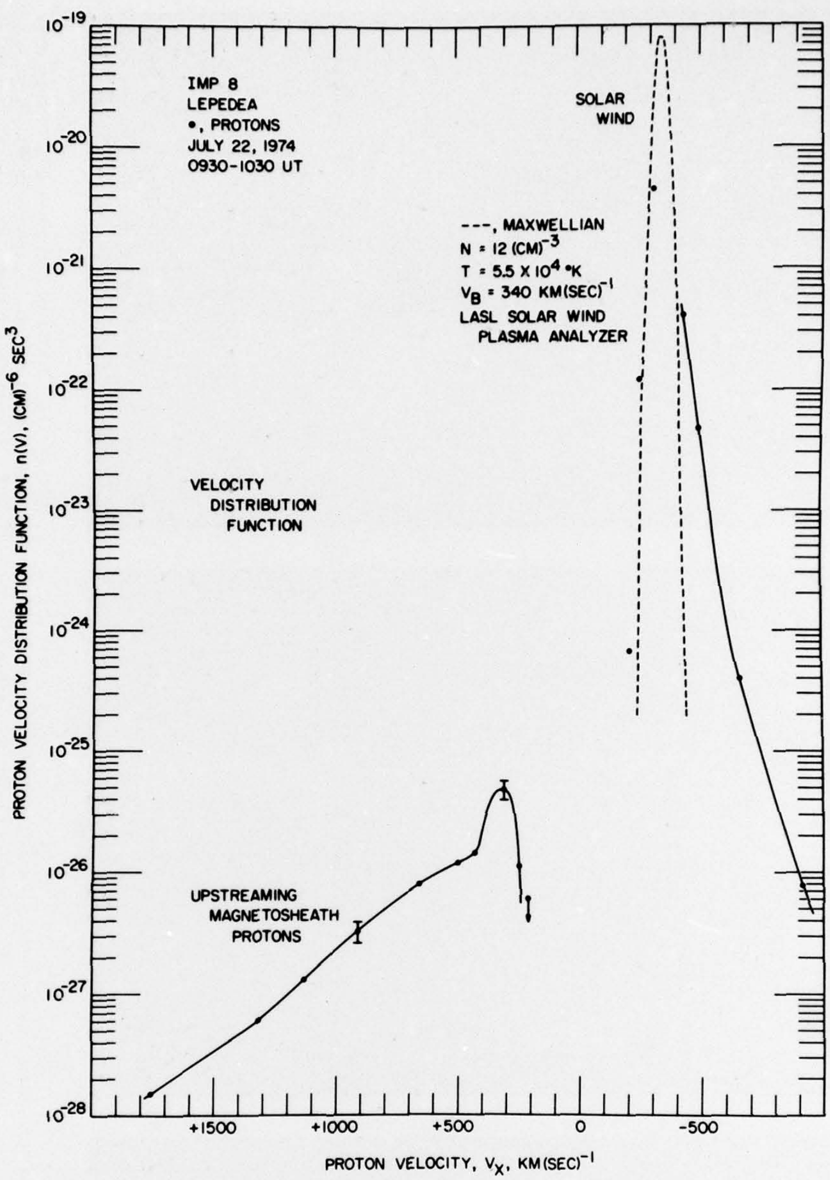

Fig. 11. Distribution function for the intense burst of protons observed streaming into the solar wind from the earth's bow shock from 0930 to 1030 UT in Plate 1. The $+V_x$ velocity axis is directed toward the sun. The dashed line gives the solar wind proton distribution function as determined from the Los Alamos plasma analyzer on Imp 8.

instability, no method was available to distinguish clearly between these two modes of propagation.

One way of distinguishing the Buneman mode from the ion acoustic mode is to measure the wavelength. The two modes differ fundamentally in the wavelengths required to account for the observed frequency spectrums. Since ion acoustic waves only occur at frequencies less than f_p^+ in the rest frame of the plasma, large Doppler shifts and correspondingly short wavelengths of tens to hundreds of meters are required to account for the frequency range, $(2\text{–}10)f_p^+$, in which the noise is usually observed. The Buneman mode, on the other hand, occurs at a frequency $f_B \simeq 3.49 f_p^+$, which requires no Doppler shift to account for the observed frequency spectrum, implying wavelengths of several hundred meters or more.

Since only a single electric dipole antenna is used on Helios, the wavelength cannot be determined. However, the Imp 6 spacecraft, which also detects the same waves upstream of the bow shock, has two antennas of different lengths which can be used to estimate wavelengths. The technique used consists of comparing the measured antenna voltages V with the tip-to-tip lengths L of the antennas. For wavelengths longer than the antenna the antenna voltage is directly proportional to the antenna length, so that the computed electric field strength $E = 2V/L$ is the same for both antennas. However, for wavelengths λ comparable to or shorter than the antenna this proportionality no longer holds. In general, we expect that when $\lambda \lesssim L$, the measured electric field strength will be underestimated.

On Imp 6 the electric field antennas consist of two orthogonal dipoles with tip-to-tip lengths of L_y = 92.5 m and L_x =

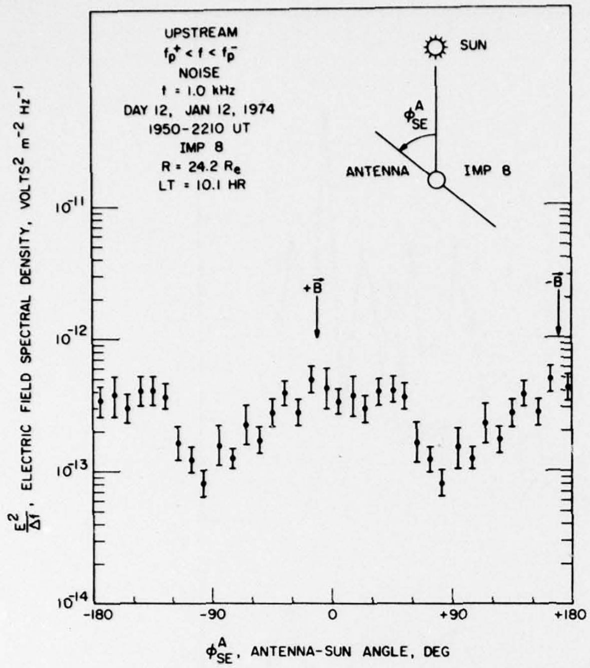

Fig. 12. Angular distribution of the electric field intensity for a burst of $f_p^+ < f < f_p^-$ noise produced by upstreaming magnetosheath protons. These data show that the electric field of the proton-driven $f_p^+ < f < f_p^-$ noise is parallel to the solar wind magnetic field, essentially identical to the $f_p^+ < f < f_p^-$ noise detected by Helios far from the earth (compare with Figure 4).

53.5 m [*Gurnett*, 1974]. The two antennas are mounted orthogonally to each other and to the spacecraft spin axis. The spin axis is directed normal to the ecliptic plane. Simultaneous measurements of the voltage spectrums from the two antennas are made with two identical spectrum analyzers. Because of their orientation the two antennas do not detect the same component of the electric field. However, for a steady state wave spectrum, comparisons can be made by averaging over many rotations of the spacecraft.

A case for which the wavelength of the interplanetary $f_p^+ < f < f_p^-$ noise has been estimated by using this technique is shown in Figure 15. During this period, Imp 6 is upstream of the bow shock at geocentric radial distances from about 19 to 26 R_E and local times from about 9.8 to 10.2 hours. A substantial level of $f_p^+ < f < f_p^-$ noise is present during this period. Some of these events can be associated with low-energy protons arriving from the bow shock, whereas other events, such as the intense bursts from about 0520 to 0610 UT, are of interplanetary origin. This period of enhanced activity occurs shortly after an abrupt increase in the solar wind density at about 0500 UT (see the top panel of Figure 15), which preceded the onset of a high-speed solar wind stream a few hours later (W. Feldman, personal communication, 1977).

The electric field spectrums obtained from the E_y and E_x antennas during the interval from about 0530 to 0602 UT are shown in the bottom panel of Figure 16. These spectrums give the median values of all of the peak intensities obtained during this interval, computed by using $E = 2V/L$. Each point represents the median of approximately 700 individual peak measurements. Because of the impulsive temporal fluctuations a large number of measurements are needed to reduce the statistical fluctuations to an acceptable level. The ratio of the E_y to the E_x field strengths, computed from these spectrums, is shown in the top panel of Figure 16, with estimates of the corresponding error limits (one standard deviation). As can be seen, the E_y/E_x ratio is approximately 1 at low frequencies, $f \lesssim 3$ kHz, but deviates substantially below 1 at high frequencies, $f \gtrsim 10$ kHz. The decrease in the E_y/E_x ratio at high frequencies indicates that the longer, E_y antenna is significantly underestimating the field strengths in comparison to the shorter, E_x antenna. This deviation of the E_y/E_x ratio indicates that wavelengths shorter than L_y = 92.5 m are being detected at frequencies above about 3 kHz.

To demonstrate the overall accuracy and reliability of this technique, a corresponding analysis was performed on a band of whistler mode plasmaspheric hiss detected in the earth's magnetosphere a few hours later. It is easily shown that the wavelengths of these whistler mode waves are very large, much larger than the dimensions of the Imp 6 electric antennas. The results of this analysis are shown in Figure 17. As can be seen, the E_y/E_x ratio stays very close to 1 at all frequencies, thereby confirming that the wavelengths are longer than the antenna length. These and many other similar comparisons for a wide variety of plasma wave phenomena demonstrate that significant deviations of the E_y/E_x ratio below 1, such as the deviation in Figure 16, are not instrumental effects and can only be attributed to wavelengths shorter than the antenna length.

Since the accuracy of the method has been confirmed, it is now of interest to compare the measurements in Figure 16 with the wavelengths to be expected if the waves are ion acoustic waves. For typical solar wind parameters $T^- \simeq 1.5 \times 10^5$ °K it is readily shown that the ion acoustic speed $C_s = (kT^-/m^+)^{1/2} \simeq 35.2$ km s^{-1} is much less than the solar wind velocity. For these conditions the frequency detected in the spacecraft frame of reference is, to a good approximation, given entirely by the Doppler shift (valid for $f \gg f_p^+$),

$$f = (V_{sw}/\lambda) \cos \theta_{kV} \qquad (1)$$

where θ_{kV} is the angle between the propagation vector $\mathbf{k}$ and the solar wind velocity $\mathbf{V}_{sw}$. Even though the ion acoustic mode can propagate at a substantial angle to the magnetic field [*Stix*, 1962], the $f_p^+ < f < f_p^-$ noise is evidently generated with $\mathbf{k}$ vectors nearly parallel to the static magnetic field, since the electric field is always observed to be nearly parallel to the static magnetic field. Thus θ_{kV} can be determined from the measured magnetic field direction; i.e., $\theta_{kV} \simeq \theta_{BV}$. By solving (1) for λ by means of the appropriate solar wind speed $V_{sw} \simeq 360$ km s^{-1} from Figure 15 and by means of $\theta_{BV} \simeq 22°$ from the Imp 6 magnetometer data (D. Fairfield, personal communication, 1977) the wavelengths corresponding to each frequency can be calculated. These wavelengths are shown by the wavelength scale at the top of Figure 16 along with the lengths L_y and L_x of the two electric antennas. As can be seen, the E_y/E_x ratio starts to deviate below 1 as soon as the computed wavelength becomes significantly shorter than the antenna. These comparisons show that the wavelength computed from the Doppler shift formula is in excellent quantitative agreement with the wavelength estimated from the E_x/E_y ratio ($\lambda \simeq 92.5$ m at $f \simeq 3$ kHz).

Further evidence of short wavelengths is provided by the upper cutoff of the observed frequency spectrum and the variation of this cutoff with radial distance from the sun. It is well known that the shortest wavelength which can occur in a plasma is determined by the onset of strong Landau damping

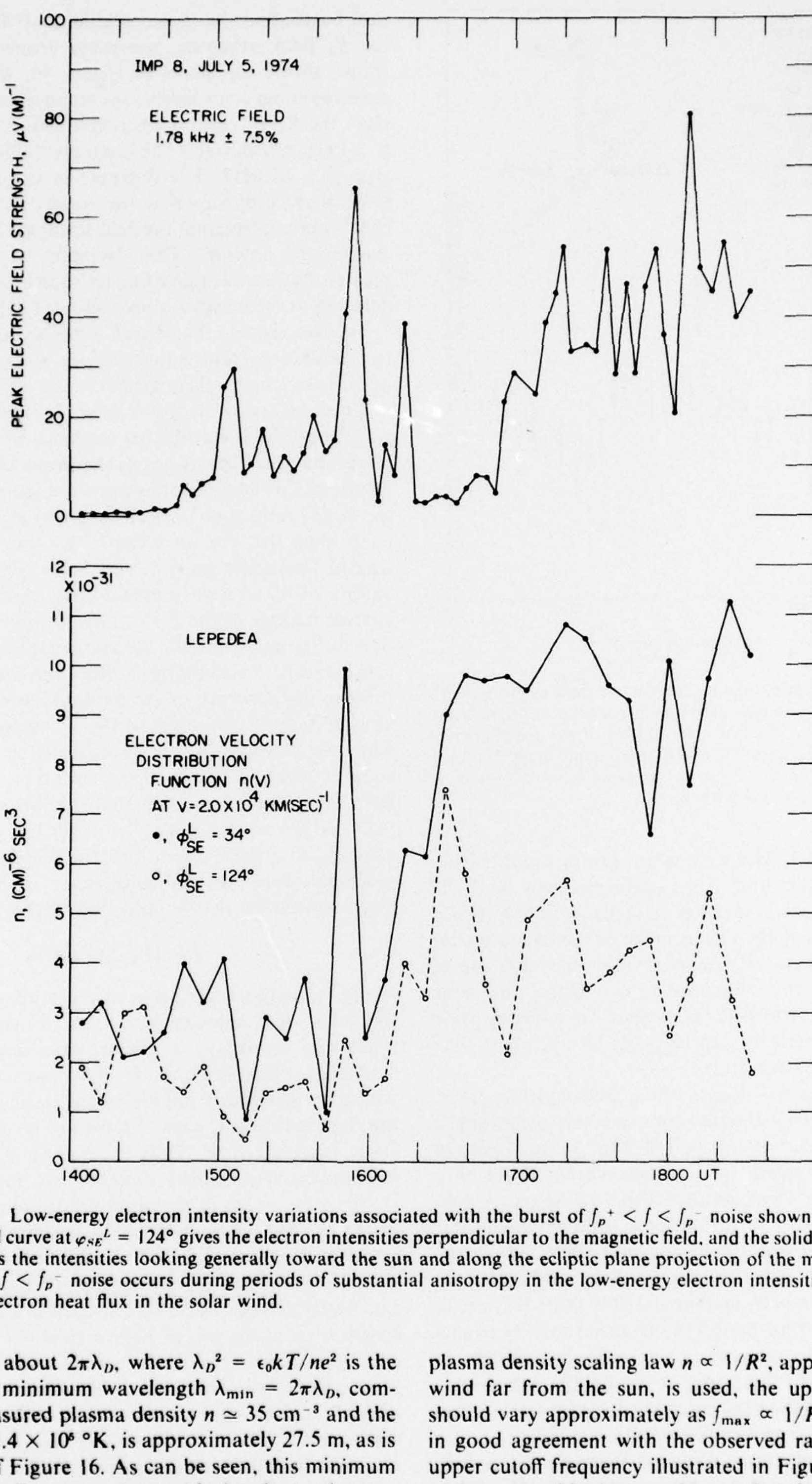

Fig. 13. Low-energy electron intensity variations associated with the burst of $f_p^+ < f < f_p^-$ noise shown in Figure 10. The dashed curve at $\varphi_{SE}^L = 124°$ gives the electron intensities perpendicular to the magnetic field, and the solid curve at $\varphi_{SE}^L = 34°$ gives the intensities looking generally toward the sun and along the ecliptic plane projection of the magnetic field. The $f_p^+ < f < f_p^-$ noise occurs during periods of substantial anisotropy in the low-energy electron intensities associated with the electron heat flux in the solar wind.

at a wavelength of about $2\pi\lambda_D$, where $\lambda_D^2 = \epsilon_0 kT/ne^2$ is the Debye length. The minimum wavelength $\lambda_{min} = 2\pi\lambda_D$, computed from the measured plasma density $n \simeq 35$ cm^{-3} and the temperature $T^- = 1.4 \times 10^5$ °K, is approximately 27.5 m, as is shown at the top of Figure 16. As can be seen, this minimum wavelength is in excellent agreement with the observed upper cutoff frequency of the electric field spectrum. The dependence of the minimum wavelength on the plasma density, $\lambda_{min} \propto \lambda_D \propto 1/n^{1/2}$, furthermore explains the tendency for the upper cutoff frequency $f_{max} \simeq (V_{sw}/\lambda_{min}) \propto n^{1/2}$ to increase with decreasing radial distance from the sun (see Figure 6), since the plasma density increases closer to the sun. When the plasma density scaling law $n \propto 1/R^2$, appropriate for the solar wind far from the sun, is used, the upper cutoff frequency should vary approximately as $f_{max} \propto 1/R$, which is seen to be in good agreement with the observed radial variation of the upper cutoff frequency illustrated in Figure 6. All these comparisons provide strong evidence that the low-frequency electrostatic waves detected in the solar wind by Imp 6, Imp 8, and Helios have short wavelengths and Doppler shifts consistent with the identification of these waves as ion acoustic waves.

Although short wavelengths are clearly evident for the event in Figure 16, in most cases the $f_p^+ < f < f_p^-$ noise detected by Imp 6 does not show these effects. The event in Figure 16 is

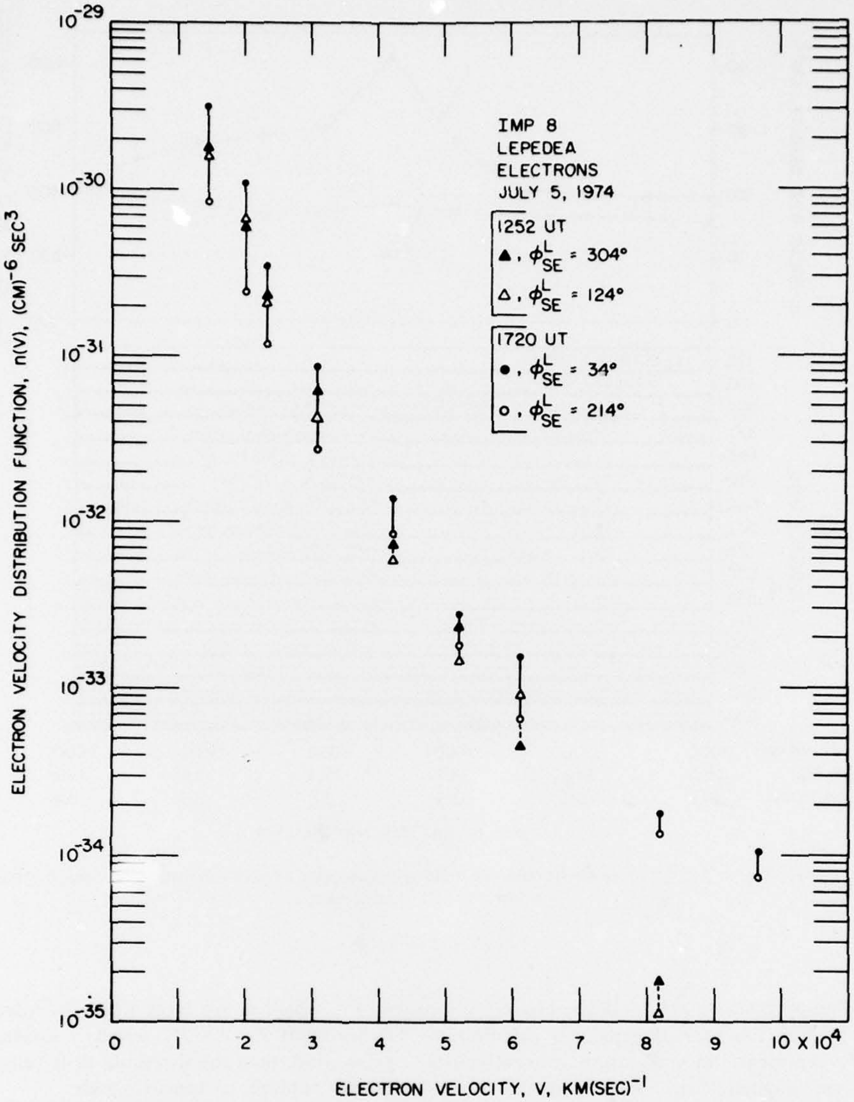

Fig. 14. Further details of the anisotropic electron distribution associated with the burst of $f_p^+ < f < f_p^-$ noise shown in Figure 10, selected for times when the magnetic field is aligned parallel to the viewing direction of the Lepedea. At 1252 UT the anisotropy is very small, and no $f_p^+ < f < f_p^-$ noise is present. At 1720 UT the anisotropy is large, particularly at the lower velocities, and the $f_p^+ < f < f_p^-$ noise intensities are correspondingly large.

unusual in that the plasma density is very large, $n = 35$ cm^{-3}, and results in a minimum wavelength substantially less than the antenna length. For typical solar wind plasma densities at 1 AU, $n \simeq 5$ cm^{-3}, the minimum wavelength is approximately $\lambda_m = 72$ m, which is evidently sufficiently large to make short-wavelength effects undetectable even though wavelengths shorter than the Imp 6 antenna length, $L_v = 92.5$ m, could occur. Note from Figure 16 that most of the wave energy occurs at wavelengths substantially larger than $\lambda_{min} = 2\pi\lambda_D$ and that the intensity is strongly attenuated for wavelengths approaching λ_{min}. It should also be noted that because of the shorter length of the Helios antennas ($L = 16$ m for Helios 1, and $L = 32$ m for Helios 2), errors due to short-wavelength effects are not normally expected to be significant for the Helios measurements, except for unusually high densities.

ORIGIN OF THE SOLAR WIND ION ACOUSTIC WAVES

Having established that the $f_p^+ < f < f_p^-$ noise consists of short-wavelength ion acoustic waves, we now consider the mechanisms for generating these waves, both in the interplanetary medium and in the region upstream of the bow shock. The observed triggering of the ion acoustic waves by an increase in the electron heat flux provides strong evidence that the ion acoustic mode is being driven unstable by the electron heat flux in the solar wind, as was first suggested by *Forslund* [1970].

The basic mechanism proposed by *Forslund* [1970] is illustrated schematically in Figure 18, which shows the general form of the reduced one-dimensional electron and proton distribution functions in the solar wind. The reduced one-

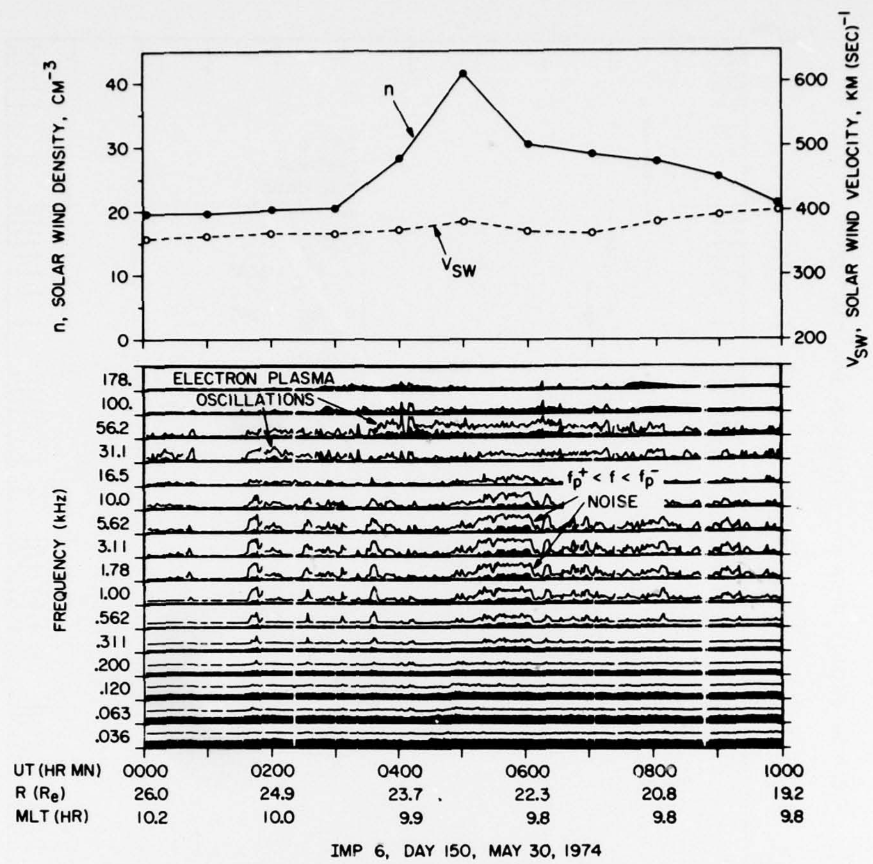

Fig. 15. Series of $f_p^+ < f < f_p^-$ noise bursts detected by Imp 6 in association with a density compression preceding a high-speed solar wind stream.

dimensional distribution function $F(V)$ is defined by $F(V) = \int d\mathbf{V}_\perp f(\mathbf{V})$, where $f(\mathbf{V})$ is the three-dimensional distribution function and $d\mathbf{V}_\perp$ represents an integration over velocities perpendicular to the magnetic field. As is indicated, a substantial anisotropy is produced in the high-energy, or 'halo,' electrons by the electron heat flux flowing outward away from the sun [*Feldman et al.*, 1974, 1975]. Since the net current in the solar wind is essentially zero, except at discontinuities, the electron current associated with the antisunward drift of the energetic 'halo' electrons must be compensated by a sunward drift of the low-energy 'core' electrons. This drift velocity V_d is indicated in Figure 18. If the double peak in the combined velocity distribution function $F(V) = F^-(V) + (m^-/m^+)F^+(V)$ produced by this drift is sufficiently large, then the ion acoustic mode is unstable. Since the drift is parallel to the static magnetic field, the waves produced by this instability are expected to have their wave vectors and electric fields oriented approximately parallel to the static magnetic field. The condition for instability is given by the Penrose criterion

$$\int_{-\infty}^{\infty} \frac{F(V) - F(V_0)}{(V - V_0)^2}\, dV > 0 \qquad (2)$$

where V_0 is the velocity of the minimum in $F(V)$ [*Penrose*, 1960]. For equal electron and ion temperatures $T^- \simeq T^+$ the threshold drift velocity is very large, approximately $V_t = (kT^-/m^-)^{1/2}$, which is too large to be exceeded in the solar wind. However, if $T^- \gg T^+$, which is sometimes satisfied in the solar wind, then the threshold drift velocity for instability is greatly reduced, to approximately

$$V_t \simeq (kT^+/m^+)^{1/2} \qquad (3)$$

[*Krall and Trivelpiece*, 1973]. For a solar wind ion temperature of $T^+ \simeq 4.0 \times 10^4$ °K the threshold drift velocity is, for example, only $V_t = 18$ km s^{-1} ($T^- \gg T^+$ being assumed). For electron temperatures only moderately larger than the ion temperature the threshold drift velocity is larger than (3) by a factor which depends on T^-/T^+ [see *Krall and Trivelpiece*, 1973]. On the basis of his analysis, *Forslund* [1970] concluded that the ion acoustic mode should be driven unstable by the electron heat flux whenever the electron to ion temperature ratio is sufficiently large.

Both the observed electric field orientation and the association of enhanced ion acoustic wave activity with increases in the electron anisotropy provide substantial evidence for the mechanism proposed by *Forslund* [1970]. The detailed arguments in support of this mechanism are, however, more involved, since all other types of double-peak distribution functions which could possibly generate ion acoustic waves must be eliminated from consideration. Charged particle measurements, such as those in Plates 2 and 3, clearly show that ion

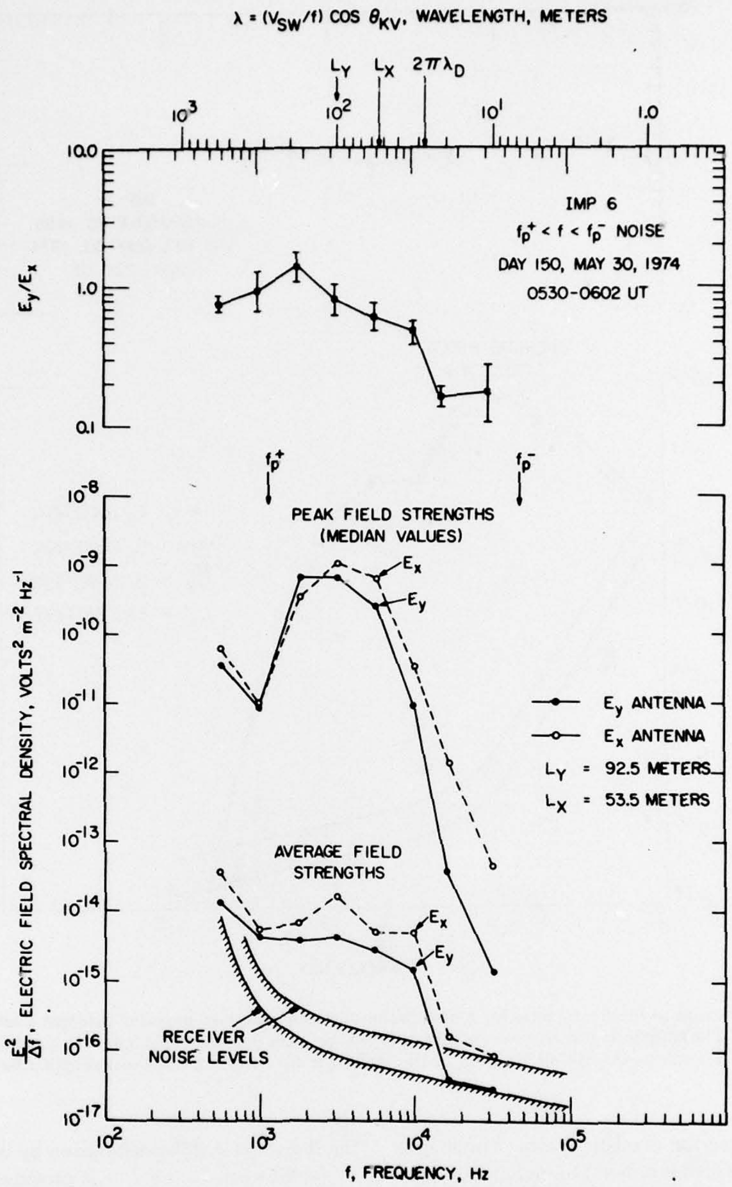

Fig. 16. Comparison of the electric field amplitudes for the burst of $f_p^+ < f < f_p^-$ noise from 0530 to 0602 UT in Figure 15 using antennas of two different lengths. The deviation of the E_y/E_x ratio below 1 indicates that the wavelengths of the waves are shorter than the longest antenna, L_y = 92.5 m, at frequencies above about 3 kHz. The scale at the top of the illustration indicates the wavelength which would occur if the observed frequencies were entirely due to Doppler shifts. Note the close correspondence of the upper frequency cutoff to the minimum wavelength $2\pi\lambda_D$ caused by Landau damping.

acoustic waves occur during times when no secondary peak is detectable in either the electron or the proton distribution functions, within the energy range (50 eV $\lesssim E \lesssim$ 45 keV) and resolution of the Lepedea. Although electron energies less than 100 eV were not investigated, it is almost completely certain, on the basis of the results of *Feldman et al.* [1975], that double peaks do not occur in the electron distribution function at energies less than 100 eV. It is possible that closely spaced double peaks could occur in the ion distribution, such as the double proton streams reported by *Feldman et al.* [1973*a*], and still be unresolved in the Lepedea data. Comparisons with published examples of double proton streams [*Feldman et al.*, 1973*a*] do not show a close correspondence with the occurrence of ion acoustic waves; however, further detailed studies are needed to investigate whether double proton streams can under some circumstances generate ion acoustic waves. On the assumption that the ion distribution functions do not generally have the double-peaked form required to produce an instability, essentially the only possibility left is the double peak produced by a velocity shift between the peaks in the electron and ion distributions, as illustrated in Figure 18. The presence of such a velocity shift in the solar wind has now been amply demonstrated by *Feldman et al.* [1974, 1975]. It only remains to be demonstrated that this shift is sufficiently large to exceed

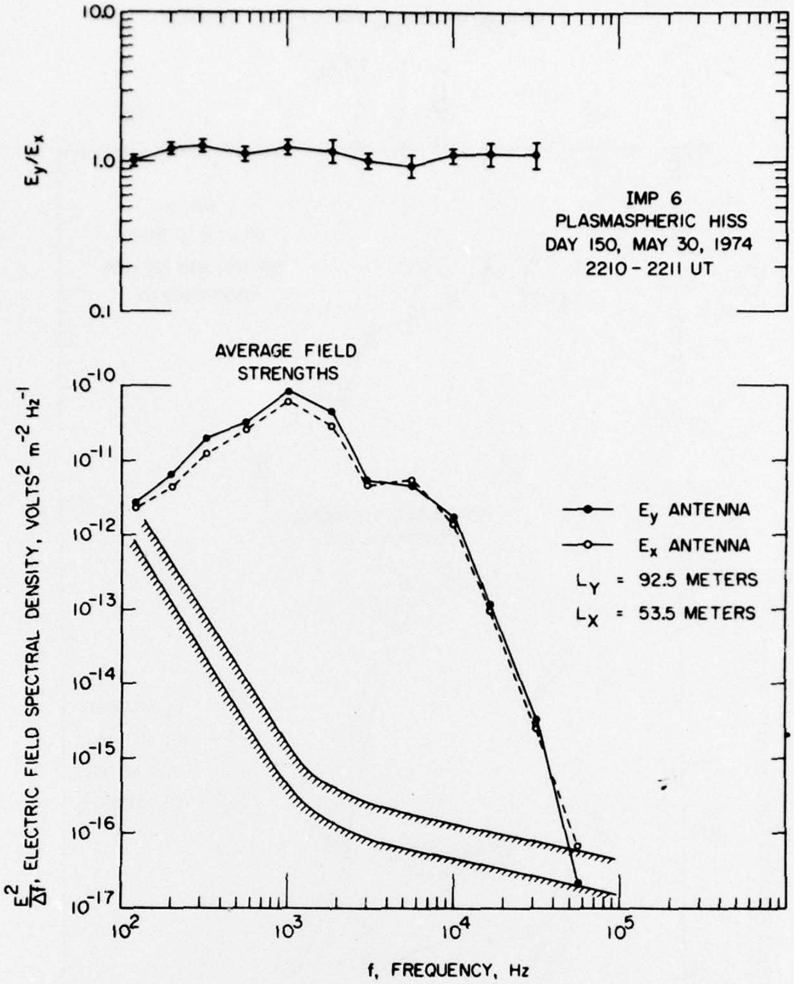

Fig. 17. Comparison of the E_y/E_x ratio for a broadband plasmaspheric hiss emission observed a few hours after the event in Figure 16. Plasmaspheric hiss has wavelengths much longer than the antenna length. The close correspondence of the E_y/E_x ratio to 1 confirms the overall accuracy of this technique for detecting short-wavelength effects.

the threshold for generating ion acoustic waves. The magnitude of the velocity shift, which is difficult to measure directly, can be estimated from the anisotropy in the halo electron distribution. For the event in Figure 14 at 1720 UT the flux of electrons along the magnetic field (first moment) is estimated to be 1.50×10^8 el (cm^2 s)$^{-1}$. When the measured local plasma density of $n = 10.1$ el cm^{-3} is used, this flux must be compensated by a sunward drift of the core electrons at a velocity of about 150 km s^{-1}. The ratio of this drift velocity to the electron thermal speed ($T^- = 1.5 \times 10^5$ °K being used) is about 0.1. Whether this drift velocity exceeds the threshold drift velocity for the ion acoustic wave instability is critically dependent on the electron to ion temperature ratio. For the period of interest the ion temperature measured by the Los Alamos plasma probe on Imp 8 is $T^+ = 7.1 \times 10^4$ °K. When a typical temperature of $T^- = 1.5 \times 10^5$ °K is used for the core electrons, the temperature ratio is $T^-/T^+ = 2.14$. For this relatively low electron to ion temperature ratio the ion acoustic mode should be stable according to the curves given by *Stringer* [1964]. On the other hand, if a typical halo temperature of $T^- = 7.0 \times 10^5$ °K is used, which gives $T^-/T^+ = 10$, the threshold drift velocity given by equation (3), $V_t = 23$ km s^{-1} (valid when $T^- \gg T^+$), is exceeded by a substantial factor. Since no computer calculations of the threshold drift velocity are available for a realistic combination of core and halo electron distributions, the stability of the ion acoustic mode cannot be accurately determined. However, since the correct effective electron to ion temperature ratio is probably somewhere in between the two extremes given by the core and halo temperatures, it seems likely that the ion acoustic mode is unstable in this case. Further detailed analyses of the exact instability conditions are needed for realistic models of the solar wind electron distribution to answer this question clearly.

For the ion acoustic waves generated by protons streaming into the solar wind from the bow shock there is no question about which particles are responsible for the instability. However, considerable uncertainty still remains concerning the detailed mechanism by which the proton stream produces the instability. In considering the origin of the instability, two distinctly different mechanisms can be identified: (1) the instability may be caused directly by the double peak in the proton

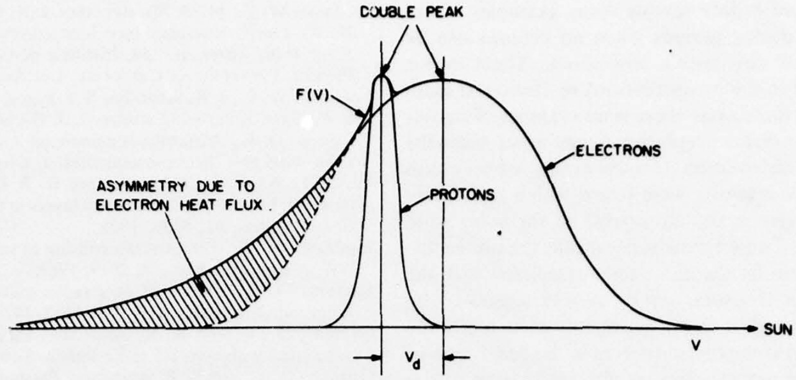

Fig. 18. Illustration showing the velocity shift V_d between the low-energy electrons and the solar wind protons, required to maintain zero net current when a substantial electron heat flux is present. If the velocity shift is sufficiently large, the resulting double peak in the combined electron and proton distribution function $F(V)$ can cause the ion acoustic mode to become unstable.

distribution (see Figure 11), or (2) the instability may be caused indirectly by the shift in the velocity of the core electrons required to maintain zero net current, similar to the heat flux mechanism. Of these two possibilities the second mechanism is believed to be dominant. For the first mechanism, rough estimates show that the peak in the proton distribution function due to the upstreaming protons is simply too small to be unstable according to the Penrose criterion. Note that the contribution of the proton stream to $F(V)$ is greatly reduced by the factor (m^-/m^+) in the combined one-dimensional distribution function, in addition to the fact that the distribution function for this stream is nearly 6 orders of magnitude below the peak due to the solar wind beam (see Figure 11). On the other hand, the proton flux associated with the upstreaming protons can be quite substantial, $\sim 5 \times 10^6$ protons $(cm^2\ s)^{-1}$. The upstreaming protons must therefore cause a shift in the velocity of the core electrons with respect to the solar wind protons in order to maintain zero net current. If this shift is large enough to produce instability, this mechanism will explain why the ion acoustic waves driven by the upstreaming protons are so similar to the interplanetary ion acoustic waves, since the mechanisms are essentially identical. Note that halo electrons streaming away from the sun and sunward streaming protons both contribute in the same sense to the current imbalance. Detailed comparisons, however, often show that the intensities of the upstreaming protons are too small, by factors of 10–100, to produce velocity shifts exceeding the threshold for the ion acoustic wave instability using a simple Maxwellian distribution for the core electrons. The detailed explanation of this discrepancy is not known; however, one possibility is that the electron heat flux maintains the plasma near marginal stability for ion acoustic waves, so that only a small current imbalance is needed to trigger the instability. Also, *Feldman et al.* [1973*b*] have shown that protons streaming into the solar wind from the earth's bow shock produce substantial perturbations in the ambient solar wind electron distribution. These perturbations and their effect on the instability condition given by the Penrose criterion must be studied in greater detail before the generation mechanism of the upstream ion acoustic waves can be completely resolved.

Numerous investigators have suggested possible roles which ion acoustic turbulence may play in determining the large-scale properties of the solar wind. It has been suggested that plasma waves can heat the solar wind ions [*Fredricks*, 1969], regulate the electron heat flux in the solar wind [*Forslund*, 1970; *Schulz and Eviatar*, 1972], and thermally couple the electron and ion distributions [*Perkins*, 1973]. The extent to which the ion acoustic waves detected by Helios and Imp 6 and 8 play any significant role in these processes remains to be determined. At 1 AU the maximum intensities of the ion acoustic turbulence are relatively small, energy density ratios being approximately $\epsilon_0 E^2/2nkT \simeq 10^{-6}$. The turbulence is, however, present a large fraction of the time and increases rapidly in intensity with decreasing radial distance from the sun. These factors all suggest that the presence of these waves must be given serious consideration in the overall understanding of the solar wind, particularly in relation to the regulation of the solar wind heat flux.

SUMMARY AND CONCLUSION

Plasma wave measurements on the solar-orbiting Helios spacecraft have previously shown that sporadic bursts of electrostatic turbulence are commonly observed in the solar wind at frequencies between the electron and ion plasma frequencies [*Gurnett and Anderson*, 1977]. In this paper we have expanded the earlier investigation of these waves using the Helios data and have compared the Helios results with similar measurements from the earth-orbiting Imp 6 and 8 spacecraft. Wavelength measurements with the Imp 6 spacecraft now provide strong evidence that these waves are short-wavelength ion acoustic waves at $f \lesssim f_p^+$ which are Doppler-shifted upward in frequency by the motion of the solar wind. The upper cutoff frequency and the variation of this cutoff frequency with radial distance from the sun, $f_{max} \propto 1/R$, are in close agreement with the short-wavelength cutoff expected for ion acoustic waves.

Comparison with the Imp 6 and 8 data reveals that a substantial fraction, 50–70%, of the ion acoustic wave turbulence detected in the solar wind near the earth is caused by suprathermal protons streaming into the solar wind from the earth's bow shock. These waves, which correspond to the upstream electrostatic waves first reported by *Scarf et al.* [1970], are observationally indistinguishable from the ion acoustic waves detected by Helios. Although both the upstream proton-driven waves and the waves detected by Helios are evidently ion acoustic waves, some distinctly different source is required to explain the Helios observations, since protons from the earth's bow shock cannot possibly account for the waves detected by Helios far from the earth. Examination of the Imp 6 and 8 data reveals many examples of ion acoustic turbulence during periods when no protons can be detected coming from the earth's bow shock. These events evidently correspond to the waves detected by Helios far from the earth. Usually in these cases there is no evidence of significant suprathermal electron or proton fluxes other than the quiescent solar wind distribution. In a few events, variations in the ion acoustic wave intensity were found which are closely correlated with changes in the anisotropy of the solar wind electron distribution. These events suggest that the ion acoustic turbulence is driven by the anisotropy associated with the electron heat flux in the solar wind, as was suggested by *Forslund* [1970]. Although it seems reasonably certain that the electron heat flux is in some cases involved in the generation of the interplanetary ion acoustic waves, the association of ion acoustic waves with suprathermal protons from the bow shock suggests that the solar wind ion distributions should be investigated in greater detail to see if double ion streams and other nonthermal solar wind ion distributions could also be involved in the generation of these waves.

Acknowledgments. The authors express their thanks to William Feldman from the Los Alamos Scientific Laboratory for providing the Imp 8 plasma density and temperature measurements used in this report. The research at the University of Iowa was supported in part by NASA under contracts NAS5-11279, NAS5-11431, and NAS5-11064 and grants NGL-16-001-002 and NGL-16-001-043 and by the Office of Naval Research.

The Editor thanks W. Bernstein and F. L. Scarf for their assistance in evaluating this paper.

REFERENCES

Buneman, O., Instability, turbulence and conductivity in a current-carrying plasma, *Phys. Rev. Lett.*, *1*, 8, 1958.

Feldman, W. C., J. R. Asbridge, S. J. Bame, and M. D. Montgomery, Double ion streams in the solar wind, *J. Geophys. Res.*, *78*, 2017, 1973*a*.

Feldman, W. C., J. R. Asbridge, S. J. Bame, and M. D. Montgomery, Solar wind heat transport in the vicinity of the earth's bow shock, *J. Geophys. Res.*, *78*, 3697, 1973*b*.

Feldman, W. C., M. D. Montgomery, J. R. Asbridge, S. J. Bame, and H. R. Lewis, Interplanetary heat conduction—Imp 7 results, in *Solar Wind Three*, p. 334, Institute of Geophysics and Planetary Physics, University of California, Los Angeles, Calif., 1974.

Feldman, W. C., J. R. Asbridge, S. J. Bame, M. D. Montgomery, and S. P. Gary, Solar wind electrons, *J. Geophys. Res.*, *80*, 4181, 1975.

Forslund, D. W., Instabilities associated with heat conduction in the solar wind and their consequences, *J. Geophys. Res.*, *75*, 17, 1970.

Frank, L. A., K. L. Ackerson, and R. P. Lepping, On hot tenuous plasmas, fireballs, and boundary layers in the earth's magnetotail, *J. Geophys. Res.*, *81*, 5859, 1976.

Fredricks, R. W., Electrostatic heating of solar wind ions beyond 0.1 AU, *J. Geophys. Res.*, *74*, 2919, 1969.

Gurnett, D. A., The earth as a radio source: Terrestrial kilometric radiation, *J. Geophys. Res.*, *79*, 4227, 1974.

Gurnett, D. A., and R. R. Anderson, Electron plasma oscillations associated with type III radio bursts, *Science*, *194*, 1159, 1976.

Gurnett, D. A., and R. R. Anderson, Plasma wave electric fields in the solar wind: Initial results from Helios 1, *J. Geophys. Res.*, *82*, 632, 1977.

Gurnett, D. A., and L. A. Frank, The relationship of electron plasma oscillations to type III radio emission and low-energy solar electrons, *Solar Phys.*, *45*, 477, 1975.

Krall, N. A., and A. W. Trivelpiece, *Principles of Plasma Physics*, p. 482, McGraw-Hill, New York, 1973.

Penrose, O., Electrostatic instability of a uniform non-Maxwellian plasma, *Phys. Fluids*, *3*, 258, 1960.

Perkins, F., Heat conduction, plasma instabilities, and radio star scintillations in the solar wind, *Astrophys. J.*, *179*, 637, 1973.

Scarf, F. L., R. W. Fredricks, L. A. Frank, C. T. Russell, P. J. Coleman, Jr., and M. Neugebauer, Direct correlations of large-amplitude waves with suprathermal protons in the upstream solar wind, *J. Geophys. Res.*, *75*, 7316, 1970.

Schulz, M., and A. Eviatar, Electron-temperature asymmetry and the structure of the solar wind, *Cosmic Electrodynamics*, *2*, 402, 1972.

Stix, T. H., *The Theory of Plasma Waves*, p. 215, McGraw-Hill, New York, 1962.

Stringer, T. E., Electrostatic instabilities in current-carrying and counterstreaming plasmas, *Plasma Phys.*, *6*, 267, 1964.

(Received April 4, 1977;
accepted August 1, 1977.)

END

DATE
FILMED

7-78

DDC

AD-A054 860 IOWA UNIV IOWA CITY DEPT OF PHYSICS AND ASTRONOMY F/G 3/2
ION ACOUSTIC WAVES IN THE SOLAR WIND,(U)
APR 77 D A GURNETT, L A FRANK N00014-76-C-0016
UNCLASSIFIED NL

2 of 2
AD A 054860

END
DATE
FILMED
7-80
DTIC

SUPPLEMENTARY

INFORMATION

UNCLASSIFIED

SECURITY CLASSIFICATION OF THIS PAGE (When Data Entered)

AD-A054 860

REPORT DOCUMENTATION PAGE		READ INSTRUCTIONS BEFORE COMPLETING FORM
1. REPORT NUMBER	2. GOVT ACCESSION NO.	3. RECIPIENT'S CATALOG NUMBER
4. TITLE (and Subtitle) ION ACOUSTIC WAVES IN THE SOLAR WIND		5. TYPE OF REPORT & PERIOD COVERED Progress, January 1978
		6. PERFORMING ORG. REPORT NUMBER
7. AUTHOR(s) D. A. Gurnett and L. A. Frank		8. CONTRACT OR GRANT NUMBER(s) N00014-76-C-0016
9. PERFORMING ORGANIZATION NAME AND ADDRESS Department of Physics and Astronomy The University of Iowa Iowa City, Iowa 52242		10. PROGRAM ELEMENT, PROJECT, TASK AREA & WORK UNIT NUMBERS
11. CONTROLLING OFFICE NAME AND ADDRESS Office of Naval Research Electronics Program Office Arlington, Virginia 22217		12. REPORT DATE January 1978
		13. NUMBER OF PAGES 17
14. MONITORING AGENCY NAME & ADDRESS(if different from Controlling Office)		15. SECURITY CLASS. (of this report) UNCLASSIFIED
		15a. DECLASSIFICATION/DOWNGRADING SCHEDULE

16. DISTRIBUTION STATEMENT (of this Report)

Approved for public release; distribution unlimited.

17. DISTRIBUTION STATEMENT (of the abstract entered in Block 20, if different from Report)

18. SUPPLEMENTARY NOTES

J. Geophys. Res., Vol. 83, No. A1, 1978, pp. 58-74.

19. KEY WORDS (Continue on reverse side if necessary and identify by block number)

Ion acoustic waves
Solar wind
Wave turbulence

20. ABSTRACT (Continue on reverse side if necessary and identify by block number)

[See page following.]

DD FORM 1 JAN 73 1473 EDITION OF 1 NOV 65 IS OBSOLETE
S/N 0102-014-6601 |

UNCLASSIFIED

SECURITY CLASSIFICATION OF THIS PAGE (When Data Entered)

Plasma wave measurements on the Helios 1 and 2 spacecraft have revealed the occurrence of electric field turbulence in the solar wind at frequencies between the electron and ion plasma frequencies. Wavelength measurements with the Imp 6 spacecraft now provide strong evidence that these waves are short-wavelength ion acoustic waves which are Doppler-shifted upward in frequency by the motion of the solar wind. Comparison of the Helios results with measurements from the earth-orbiting Imp 6 and 8 spacecraft shows that the ion acoustic wave turbulence detected in interplanetary space has characteristics essentially identical to those of bursts of electrostatic turbulence generated by protons streaming into the solar wind from the earth's bow shock. In a few cases, enhanced ion acoustic wave intensities have been observed in direct association with abrupt increases in the anisotropy of the solar wind electron distribution. This relationship strongly suggests that the ion acoustic waves detected by Helios far from the earth are produced by an electron heat flux instability, as was suggested by Forslund. Possible related mechanisms which could explain the generation of ion acoustic waves by protons streaming into the solar wind from the earth's bow shock are also considered.